Degradation phenomena of Templo Pintado painted plasters

Marta Cappai[1], Francesco Delogu[1], Denise Pozzi-Escot[2], Gianella Pacheco Neyra[2], Paola Meloni[1], Giorgio Pia[1]*

[1] Dipartimento di Ingegneria Meccanica, Chimica e dei Materiali, Università degli Studi di Cagliari, Piazza d'Armi, 09123 Cagliari, Italy.

[2] Museo Pachacamac, Antigua Carretera Panamericana Sur Km. 31.5, Distrito de Lurín, Lima

* Corresponding author: Giorgio Pia, giorgio.pia@dimcm.unica.it, telephone +390706755051, fax +390706755067

Abstract

Weathering processes of Templo Pintado (Painted Temple) caused by environmental and climatic agents have been investigated in this work. The temple is part of the archaeological complex of Pachacamac, situated in a desert area of Western Peru characterized by high relative humidity, temperature, relevant winds, and remarkable solar radiation. These atmospheric conditions result in wet-dry cycles and wind erosion, eventually inducing pulverization, exfoliation, and detachment in plaster and painted surfaces. The seasonal variation of atmospheric conditions was monitored on a daily basis for five years, revealing that the seasonal cycles exhibit great similarity. Experimental results show a linear correlation between loss of material and environmental temperature. In particular, degradation increases with temperature rises. Moreover, high temperatures are combined with stronger winds and drying of materials (wet-dry cycles), which contribute to accelerating degradation kinetics.

1. Introduction

For hundreds of years, people throughout South America have walked the ancient pilgrimage routes to consult and pay homage to the oracle of Pachacamac, a deity whose wrath was capable of creating earthquakes [1]. The archaeological sanctuary of Pachacamac is located in Peru, approximately 31 km South of Lima and 2 km from the Pacific coast, in the lower part of the Lurin Valley (12°15'20.2"S 76°54'28.6"W). Covering an area of about 465 hectares, it is located on an irregular plain dominated by four rocky promontories and surrounded by different ecosystems such as the fluvial forest and the mouth of Lurin River, the coastal strip and its surroundings rich in basins and wetlands, hills and valley, and the coastal desert characterised by sandy sediments [2]. According to Köppen-Geiger climate classification, the climate of the area may be explained as BWh (hot desert climate) [3–6].

The initial settlements in the area date back to the Archaic period (5000 B.C.), but the construction of the sanctuary was begun no later than 200 A.D. during the Lima culture (200 - 600 A.D.). With the Wari culture (600 - 1100 A.D.), the area progressively developed into a religious centre able to attract a large number of pilgrims. Starting from 1100 A.D., Pachacamac became the center of power of Ychsma people and a series of administrative buildings and dwellings including pyramids with ramps and other buildings were erected. It was during this period that Pachacamac oracle reached its peak. In 1470, Pachacamac was incorporated into the Inca Empire, evolving into an important provincial capital with administrative and religious centres. The Inca Empire remained in power until 1533 A.D., when the arrival of Spaniards caused the destruction of the oracle and the gradual abandonment of the sanctuary [7]. Eventually, the sanctuary was buried by desert sand over time.

The historical richness of the site is reflected in its urban fabric and architecture. Within the sanctuary, there are currently more than 50 buildings from different eras, constructed by using different techniques and materials, which give rise to squares, streets and cemeteries, and bear witness to a great urban planning project [7,8]. A large proportion of the buildings are made of raw earth, mostly using the adobe construction technique. Additionally, square ashlars made of lutite, a shale found in the area, are also used, especially at the base of the walls [7]. At the urban level, it is crossed by two north-south and east-west roads and surrounded by three systems of boundary walls that divide the site into three sectors intended for different functions. In particular, within the first

sector, the smallest buildings housing the structures dedicated to worship are the Old Temple (200 - 600 A.D.), the Sun Temple (1470 – 1533 A.D.) and the Painted Temple (600 - 1533 A.D.) [2].

The Painted Temple represents one of the most important buildings of the sanctuary as it was the place where the oracle resided and where pilgrims went to consult it. For this reason, it was made clearly visible from afar to pilgrims arriving at the sanctuary. As shown in Fig. 1a, it was built above a natural promontory and its surfaces decorated with polychrome paintings[2]. The building has trapezoidal shape, with a rectangular floor plan measuring 120×65 metres, and it is stepped [2,9]. Currently, residual mural painting are mostly located along the steps of the North Front (FN), a picture of which is shown in Fig. 1b [10,11].

Paintings are made using the *Temple Mate* technique. The pigments, all of mineral origin and mostly available on site, were mixed with water and an agglutinative of vegetable origin [9,12]. The colour palette has 6 main colours: garnet and vermillon red, yellow ocher, pale yellow, greenish-grey and black. Pale yellow and vermilion red currently being the most abundant colours [2,13]. The background was done by using large cotton balls (*motas*) or woolen cloths to repeatedly dab the paint on the plastered wall. In their description of the surfaces of the Painted Temple, Muelle and Wells noted the presence of remnants of cotton balls adhering to the paint. Furthermore, during excavations carried out in 1938 in the steps of the FN, cotton balls soaked in the same paint as the surfaces were discovered among the findings [14]. After painting the background, the motifs were added with a brush made of strands of human hair. The decorative figures were outlined in black to make them more visible [14].

The study of the paintings has led to the recognition of three different pictorial periods. In the second and third periods, staircases were painted by a succession of red and yellow bands of approximately 2.5 m in length, within which animal, plant and human motifs were depicted [2,9,13].

Although there is not much bibliographic information on pre-Hispanic mural paintings in South America due to their fragility, Bonavia [15] mentions that it is an ancient artistic modality with a tradition in the Andean region, developing throughout all Pre-Hispanic times. Bonavia's remarkable and comprehensive registry of archaeological sites in Peru with evidence of mural painting from the Initial Period (900 BC) to the Colonial Period (1534 AD) includes sites such as Incahuasi, Huarco, Tambo Colorado, Huaca de la Centinela, Pachacamac, Armatambo, Huadca, and Mateo Salado, where evidence of murals made from red, white, and yellow minerals has been found. These were used to paint the exterior and interior of monumental buildings. During this period, the Painted

Temple of the Pachacamac Archaeological Sanctuary was constructed, considered a representative example of pictorial technology and the use of mineral pigments for mural painting in South America [12,15–21]. Bonavia mentions that "the best contribution to [the technique of manufacture] is owed to Muelle and Wells [14], who were lucky enough to find a series of important evidence in situ for the interpretation and technological reconstruction. They made their observations in Pachacamac"[15]. In this sense, the mural paintings of the Painted Temple) of Pachacamac represent one of the best examples of pre-Hispanic mural painting in South America, at least for now.

Paintings are executed on a plaster of variable thickness that exhibit stratifications from a succession of different applications that took place at different times. Indeed, paintings were renewed on numerous occasions. In some cases, they were simply refreshed, repainting the motifs or restoring them in places where they had been almost completely erased. In other cases, a thin layer of plaster was applied over and drawings were renewed or repainted [10].

In 1938, at the time of the *XXVII Congreso Internacional de Americanistas*, large-scale excavations were carried out on many archaeological sites in the Lima area, including Pachacamac, aiming at increasing the sites to be exhibited during the conference [13]. Since 1938, the paintings of the Painted Temple have been exposed to the elements without any care about conservation, which determined the loss of a large part of found drawings. Since 2008, a conservation and experimental archaeology programme has been underway to safeguard what remains of the painted surfaces. In particular, in 2010 a removable 433 m^2 bracing and shelter, shown in Fig. 1c, was built in the FN (Fig. 1d) to mitigate the aggressive weathering phenomena that threaten daily the survival of Painted Temple [10].

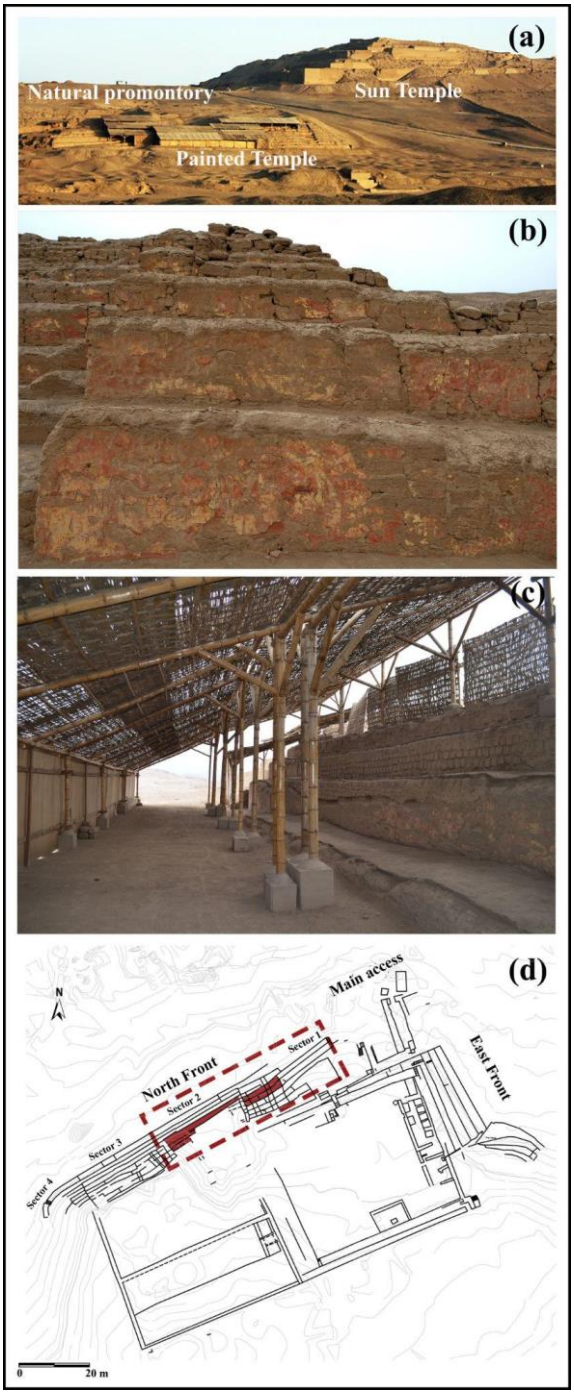

Fig. 1 - (a) Painted Temple (Image courtesy of the Santuario Arqueologico de Pachacamac); (b) FN of Painted Temple (Image courtesy of the Santuario Arqueologico de Pachacamac); (c) the shelter and bracing installed in 2010 to protect the Painted Temple; (d) sectoralisation plan for the Painted Temple (the image was adapted from D. Pozzi-Escot, G. Pacheco, C.R. Uceda, Pachacamac: Templo Pintado.Conservacion e Investigación, 2013).

Literature shows that weathering processes and their kinetics can be understood only establishing a definite relationship between the physical and chemical status of historical surfaces taking into account the variation of environmental parameters [22–28]. This is particularly important for earth-based materials, given their complexity, heterogeneity and intrinsic sensitivity to large fluctuation in temperature, relative humidity, solar radiation, wind power, salt aerosol and biovitality [29–33]. Specifically, the presence of hydrophilic phases such as clay minerals allows the material to have a high affinity to water. This last, such as liquid or atmospheric moisture, is definitely the main threat

when it comes to earthen architecture. In humid environments, even in the absence of rain, the stability of buildings is degraded by a high water content and alternating wet-dry cycles due to high temperatures or solar radiation [22,34–39].

All these factors can result in different deterioration processes such as pulverisation, exfoliation, cracking, detachments and aeolian corrasion [31,40–43], which makes conservation of archaeological earthen sites the crucial challenge of materials science applied to cultural heritage [44–47]. In this sense, constant and comprehensive monitoring of the dynamics between the environment and historical ruins, in addition to material characterization and structural analysis, is necessary to gain sufficient knowledge to plan effective strategies aimed at mitigating their rate of degradation. The study of environmental site parameters, over long periods, is certainly among the most common [36,48], along with modelling or tools like fuzzy logic approach [49,50] or GIS technologies [51]. Moreover, the aspects related to the microclimate that can specifically affect the degradation of the materials are also of considerable importance. An example is reported in Gobakken et al., in which despite the arctic climate and the resulting extreme conditions, temperatures on building materials could reach unexpected and very high values [52].

In this work, detailed information is provided on the seasonal variation of the most relevant atmospheric quantities such as solar irradiation, temperature, wind strength, and relative humidity. These quantities were measured on a daily basis for five consecutive years, obtaining a clear picture of the environmental conditions to which the painted surface of the Painted Temple is exposed. In parallel, the propensity of the painted surfaces to degradation was also monitored, measuring the mass lost from the surface when an adhesive material is gently pressed against it. It is shown that temperature is the most relevant environmental quantity affecting the cohesion of the surface layers. Additionally, the combination of relatively high temperatures and strong winds appears to give rise to the most intense degradation processes.

2. Materials and methods

2.1 Sampling and characterisation of archaeological samples

Ten samples were collected *in situ* for diagnostic investigations. The collected samples derived from a collapse that occurred in the years following the excavations of 1938 (from this date onwards, the structure was exposed without any kind of protection). These detachments have been caused to atmospheric agents and mechanical actions typical of Peruvian coast seismic phenomena. Selected samples were fragments of painted plasters in the two mostly recurrent colours in the decorations of Painted Temple: pale yellow (PY) and vermilion red (VR). Sample surfaces were

observed with a Carl Zeiss Axioscop 40 light microscope at 2.5x, 5x, 10x, 20x, 40x, and 50x magnifications. Plaster mortar (PM), PY and VR were subjected to X-ray powder diffractometry using a Rigaku MiniFlex II diffractometer and analysed by X'Pert software and Rietveld method which allows to determine primary minerals [53]. In order to identify secondary minerals (clay minerals) in-depth analysis has been carried out according to Moore et al. method [54], which consists of (i) concentrating the clay fraction, (ii) exposing it to an atmosphere saturated with ethylene glycol for 8 hours at 60 °C, and (iii) heating it in a muffle furnace at 550 °C for 2 hours. PM was characterised by wet granulometry according to UNI EN ISO 17892-4:2017 [55,56]. The particle size test on painted layers was not allowed by the smallness of samples that can be collected from the site.

2.2 Atmospheric data

Data recorded every 30 min during 5 consecutive years by the Davis Vantage Pro 2 weather station installed in the site were analysed and compared (about 17,500 readings per 5 years). Temperature (T), relative humidity (RH), wind speed (WS) and solar radiation (SR) are taken into account. Seasonal data happen to be highly homogeneous, with very small deviations. Due to the extreme uniformity of the data in the different years analysed, the five-year average was taken for each month.

2.3 Deterioration of painted surfaces

The status of painted surfaces during different seasons was carried out using the so-called scotch tape test (STT). Introduced in conservation in 1960 by Mora and Torraca [57,58] to evaluate the consolidation of stone surfaces and plasterwork, it has never been formalised through standards or norms that could provide a rigorous procedure to standardise the method and make comparable the results obtained in different studies.

At present, tapes with the adhesive on a single side or on the two sides are used [25,59–62] [63–69]. In the present work, the tape with adhesive on one side only was used. The utilization of the tape with adhesive on both sides resulted too invasive for the surfaces of Painted Temple. The test is inspired by the standard for evaluating modern coatings described in ASTM 4214-07-D and UNI EN ISO 4682-6:2011 [70,71] and adapted to the field of conservation. It is mainly used for materials with a weak degree of cohesion between the coating particles such as wall paintings [59–61] and unfired earth surfaces [62].

The 3M® Scotch® 550 polypropylene tape with acrylic adhesive was used. A 40×19 mm piece of tape was applied to the surface through a very light pressure to make it adhere to the entire area under examination as well as to eliminate any air bubbles. It was left on the surface for 90 s, removed with a constant speed of 10 mm/s at an angle of 90° and placed on a sheet with a white background. The obtained pieces of tape were scanned and processed with the free software3 ImageJ® version 1.46 and the fractional area occupied by the removed particles was evaluated. Although limited, this technique is compatible with the rules imposed by local authorities. The STT and subsequent image analysis of the tapes made it possible to estimate the material loss in archaeological surfaces.

The assessment of degradation was carried out by considering 14 portions of the step surfaces, all located on the FN in order to have a similar exposure to weathering, each measuring approximately 40 x 40 cm. Six areas on the third step and four areas on the fourth step of sector 1 were selected, as well as two areas on the fourth step and two areas on the fifth step of sector 2. Their position was established based on the colours present in order to have 7 surfaces of PY and 7 surfaces of VR.

The selected surfaces exhibited a similar state of preservation, which allows a reliable comparison. The STT was performed three times at different locations and with different tape inclinations on each surface (about 2,100 measurements per year). Measurements were taken from 12 a.m. to 3 p.m. once a month for each season. Monitoring was carried out for 2 years. The surface temperature reached by the wall paintings in different seasons was monitored using an Omega HH802 Series thermocouple. The probe was placed on a selected surface of sector 1 and another on a surface of sector 2.

3. Atmospheric data

Observations carried out on site allowed to have a clear picture of the change of weathering parameters during the times of day and months. In the coastal region of Lima, the seasonal cycle is characterized by four distinct seasons: Summer (21 December - 18 March), Autumn (19 March - 19 June), Winter (20 June - 21 September), and Spring (22 September - 20 December). In the following, we report on T, RH, SR and WS.

3.1. Temperature

The average T values during day and night are plotted in Fig. 2a for every month, while Fig. 2b repots T maximum and minimum values. In summer (southern hemisphere), particularly in

February, the average daytime T is around 21.7 °C (maximum 26 °C, minimum 18.2 °C). In winter, the daily average T, particularly in the month of August, is around 16 °C, with night-time lows equal to around 14 °C. Generally, for every month of the year, it can be seen that night and day average temperatures do not differ substantially (1±0.4 °C). Moreover, all average temperatures tend to shift towards minimum values rather than maximum values. It indicates that hotter temperatures are measured for a few hours during the day (compared to average).

3.2. Relative humidity

The average RH values plotted in Fig. 2c vary between 85.6% (May) and 93.9% (April). The variation during the day-night cycle is around 2.9% (August, average maximum 93.0%, average minimum 90.1%) and 5.6 % (March, average maximum 93.3%, average minimum 87.7%). During every month, RH reaches very high values between 99% and 97% which are the absolute maxima, while absolute minima are between 80% and 63%. A maximum daily-nightly variation of 36% has been measured during March, while minimum daily-nightly variation, measured in April and August, is 18%.

3.3. Solar radiation

As shown in Fig. 2d, SR reaches high values especially in the summer months of January, February and March. For the year analysed, the average daily radiation striking the surfaces was 7.45 kW/m^2, 7.79 kW/m^2 and 7.62 kW/m^2 respectively with peaks of 10.1 kW/m^2. The lowest SR has been recorded in August, with value of 2.89 kW/m^2. In January, SR changes from 0 to 0.791 kW/m^2 and stays on average above 0.5 kW/m^2 for three hours a day, typically from 11:00 am to 02:00 pm.

3.4. Wind speed

The average WS is plotted in Fig. 2e. It remains constant throughout the seasons at the value of 1.5 m/s ± 0.1 m/s, but in spring and summer it reaches peaks of up to 9.7 m/s. In particular, for the year under review, peaks of 7.6 m/s were reached in November. During the summer months, the average maximum WS is 5.95 m/s ± 0.25 m/s. By contrast, the lowest values were recorded during the winter months, when the average maximum speed is 3.9 m/s ± 0.25 m/s. The prevailing direction is S-SW.

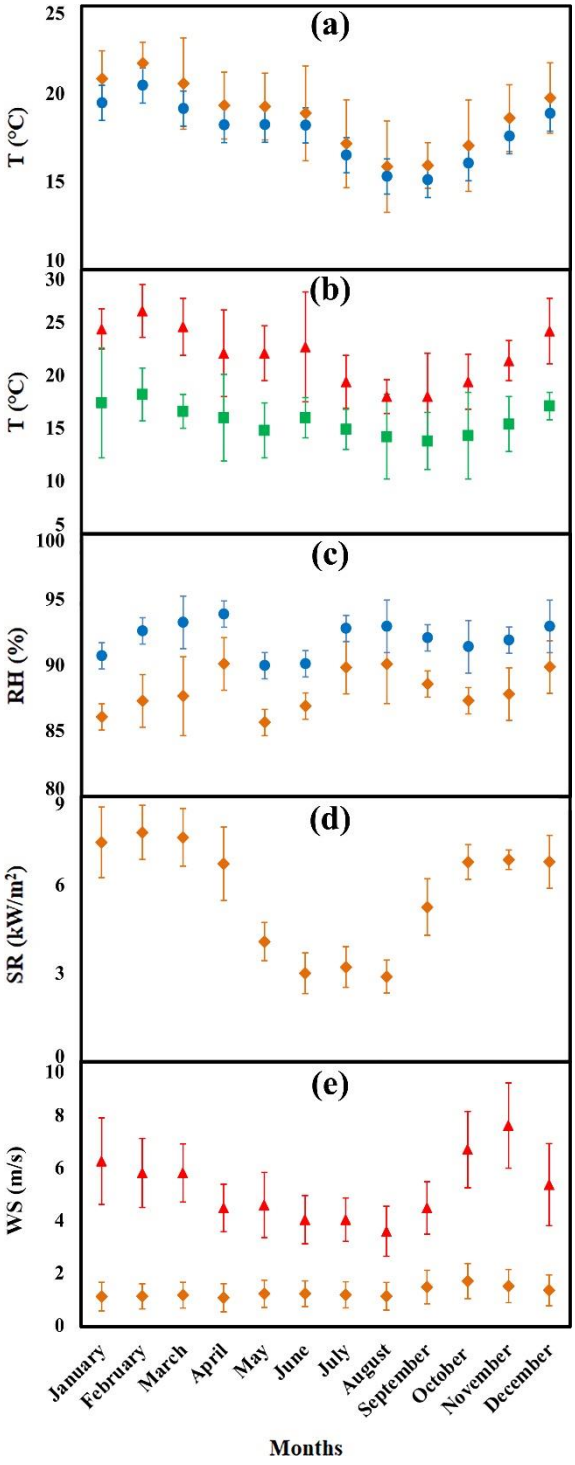

Fig. 2 - Monthly variation of (a) T (symbols: ◆ average daily T; ● average nightly T), (b) T (symbols: ▲T max; ■ T min), (c) RH (symbols: ▲ average daily RH; ■ average nightly RH), (d) SR (symbols: ◆ Average daily SR in different months), and (e) WS (symbols: ▲ WS max; ◆ average WS). The reported values represent the average of the values measured over the 5 years of monitoring.

4. Results and discussion

4.1. Characterisation of archaeological samples

Optical microscopy revealed the extreme decohesion of PY surfaces. As evident from Fig. 3a, they appear extremely pulverised. In contrast, as shown in Fig. 3b, VR surfaces appear well cohesive and the marks due to the impact of windblown sand particles are clearer. Through cross-

sectional analysis, it was possible to distinguish up to 15 pictorial layers, which vary in thickness between 10 and 200 micrometres, for a total thickness of approximately 800 micrometres (Fig. 3c).

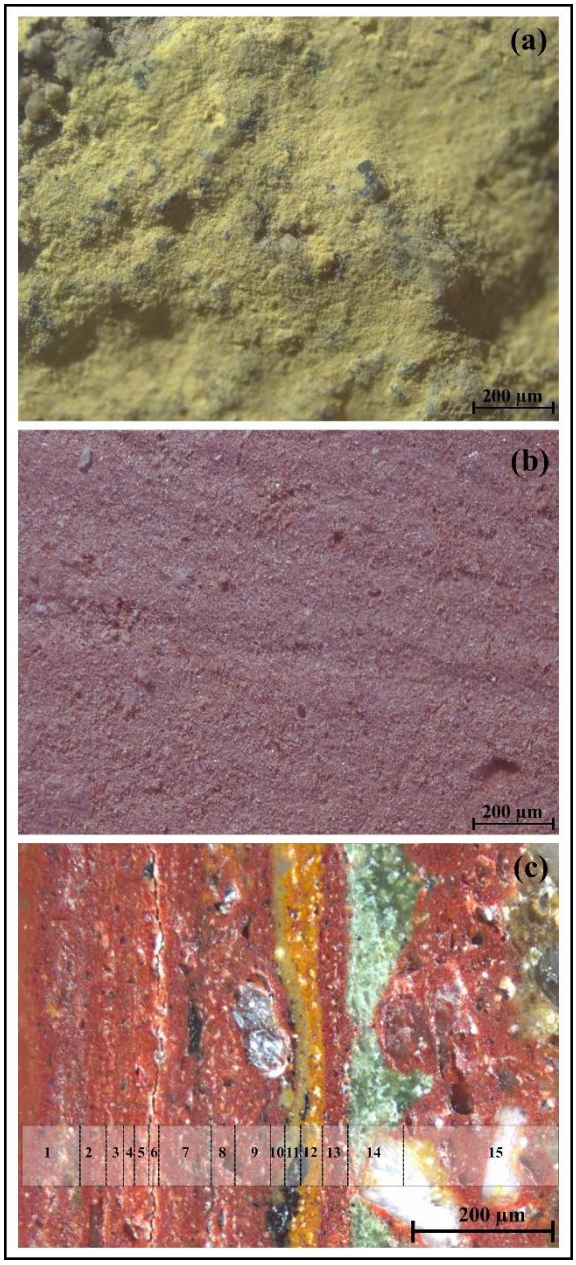

Fig. 3 - Optical microscope image of (a) PY and (b) VR surfaces. Cross-section of a painted plaster sample in which 15 pictorial layers with different thicknesses can be identified. Thicknesses - 1: 87.9 µm; 2: 37.5 µm; 3: 24.7 µm; 4: 15.5 µm; 5: 20.8 µm; 6: 14.6 µm; 7: 74.8 µm; 8: 34.3 µm; 9: 50.7 µm; 10: 21.0 µm; 11: 22.2 µm; 12: 31.6 µm; 13: 36.3 µm; 14: 80.5 µm; 15: 222.0 µm. Magnification: 5x.

The results of XRD mineralogical analysis are summarized in Tab. 1. Albite is prevalent in every mineralogical composition of analysed samples (51%, 40% and 35% in weight for PM, PY and VR respectively). Quartz is more present in VR (23%) and PM (17%), but it is less significant in PY (9%).

Tab. 1 - Mineralogical composition of the archaeological earthen plaster (PM), pale yellow (PY) and vermillon red (VR) pictorial layers.

PM	**PY**	**VR**
Albite: 51.07 ± 2.01	Albite: 40.27 ± 1.45	Albite: 35.17 ± 2.57
Clinochlore: 2.98 ± 0.12	Clinochlore: 1.90 ± 0.16	Gypsum: 1.61 ± 0.06
Hornblende: 4.33 ± 0.14	Gypsum: 0.90 ± 0.02	Hematite: 2.25 ± 0.14
Laumontite: 3.04 ± 0.42	Illite: 12.78 ± 0.80	Illite: 11.84 ± 1.95
Muscovite: 1.79 ± 0.09	Jarosite: 31.81 ± 0.84	Muscovite: 15.28 ± 4.44
Orthoclase 19.44 ± 0.98	Kozulite: 3.25 ± 0.12	Orthoclase: 6.99 ± 1.06
Quartz: 17.34 ± 0.03	Quartz: 9.08 ± 0.05	Quartz: 23.31 ± 0.07
		Riebeckite: 0.35 ± 0.03
Sigma: 2.20	Sigma: 1.93	Sudoite: 2.33 ± 0.15
Rwp%: 14.54	Rwp%: 16.70	Wollastonite: 0.86 ± 0.62
		Sigma: 1.34
		Rwp%: 9.59
Clay minerals group– qualitative identification		
Illite	Illite	Illite
Chlorite	Chlorite	Chlorite
Smectite		

The amount of clay in PM is about 3% and its qualitative interpretation reveals the presence of Smectitic Group. Jarosite quantity (32%) is responsible for the colour of PY surfaces, while the quantity of clay minerals is about 2% for the Chlorite Group and approximately 13% for Illite Group. In VR surface, the colour is attributable to the presence of 2% of hematite. About 14% is made up of Illites and Chlorites.

According to Wentworth class [72], granulometric analysis show that the plaster mixture is made up of very fine gravel (0.91%), 71.32% sand (divided in very coarse, 0.64%; coarse, 1.58%; medium, 12.45%; fine, 43.84%; and very fine, 12.81%), 27.77% silt and clay.

4.2. Correlation between deterioration rate and weathering conditions

Earth materials are characterised by highest hydrophilic phases, which are responsible for moisture and water absorption [73]. Water vapour permeability and water capillary absorption are the physical phenomena involved. Particularly in winter, RH remains approximately 100% for many hours a day. In combination with T, solar radiation and WS values, this determines water condensation on wall surfaces. Correspondingly, the absorption process is made faster. Fig. 4 shows the variation in environmental temperature (T), surface temperature (T_S) and Dew Point (DP) during critical hours of a typical winter day (from 18:00 to 9:00; the other hours of the day have not been considered because solar radiation significantly increases the temperature of the surfaces under study, which reach values incompatible with the condensation phenomenon). It can be noted

that during the time interval between approximately 3:00 am to 7:00 am, TS < DP, which means that the condensation phenomenon could occur.

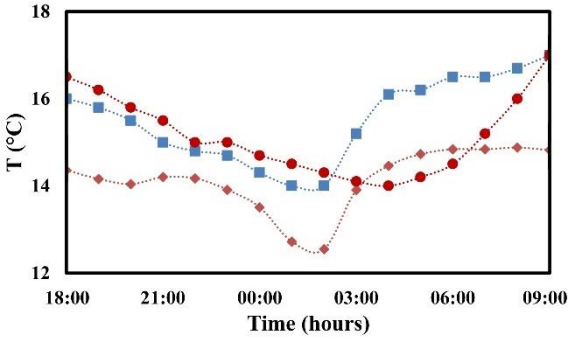

Fig. 4 - Variation of environmental temperature (T), ■; surface temperature (T_S), ●; and Dew Point (DP), ◆; *vs* critical hours of a typical winter day (from 18:00 to 9:00).

During summer, condensation is less frequent and the principal absorption process is due to water vapour penetration. In both cases, the absorbed (liquid) or condensed (vapour into the pores) water circulates into the pore network generating different conditions that can give rise to deterioration [74]. In the examined case, swelling of clay minerals is the most relevant cause of material damage.

Deterioration produced by swelling also depends on the minerals contained in the earthen mixture. In particular, the presence of minerals belonging to the Smectite Group makes this phenomenon particularly intense, resulting in deformation of plaster and all analysed painted surfaces. Furthermore, even though clay minerals belonging to the chlorite and illite groups do not swell intracrystalline upon contact with water molecules, they can still undergo osmotic (or intercrystalline) swelling as a result of bilayer interactions between clay particles, which can cause significant expansion, deformation, and associated stress in the presence of an aqueous solution [75–78]. Repeated wetting/drying cycles could lead to the development and propagation of cracks.

On the microscopic scale, bonding forces between clay particles, sand grains and silt decrease as the amount of absorbed water increases (environmental RH increase), thus reducing the internal cohesion of the material. Consequently, mechanical properties on the macroscopic scale are negatively affected [27].

The enhanced deterioration power of swelling is connected to SR (maximum values bring surfaces to highest temperatures), WS and frequency (air circulation close to surfaces). They all are able to influence evaporation and absorption cycles.

Regarding surface temperatures, measurements show an average value equal to 53 °C during the summer months, with temperature peaks of 64 °C on days when SR was most intense. The same phenomenon is analysed in the study of the degradation kinetics of the Chinese ruins of Jiaohe in China [22]. Also in such case, earthen structures are located in a semi-desert area and the dynamics involved in weathering are very similar to those of Pachacamac site. In particular, the correlation of ambient temperatures at the Jiaohe site with temperatures of the masonry pointed out that, for air temperatures between 20 °C and 30 °C, the surface temperature of buildings exceeds 50 °C.

Finally, the wind speeds up the drying of surfaces, making the cycle more deleterious in the spring and summer months when it blows with greater force, which also corresponds to the months when SR reaches its maximum, especially affecting the surfaces of the FN due to S-SW direction. Indeed, water evaporation inside porosities induces a volume contraction of clay minerals, which gives rise to microscopic and macroscopic cracks. The newly generated cracks, in turn, increase the absorption capacity of surface water during subsequent wetting cycles, with a progressive worsening of cohesion.

The stresses induced by expansion and contraction processes induce the detachment of the plaster layer from the support, which is evident in the image reported in Fig. 5a, and of the different paint layers from each other, resulting in enhanced exfoliation, especially in the case of red and greenish-grey paintings shown in Fig. 5b [79].

The importance of wind action for weathering process is not only related to the evaporation kinetics, but also to corrasion processes. Indeed, winds carry solid particles (sand, clays and organic grains) that can impact surfaces, resulting in surface abrasion and material removal [80–82]. This factor is particularly relevant in desert and semi-desert areas, such as the one of Pachacamac site [26,83–87].

The damage effect of corrasion depends on wind intensity and time of exposure. Several factors related to air (velocity, turbulence, density and viscosity), soil (composition, general morphology topographic features and humidity content) and particles carried by wind (roughness, hardness, mineralogical composition, specific gravity, characteristics diameter size and shape) play a role [25,43,88–91].

Three different modes of particle movement can be distinguished depending on the particle diameter (ø): (*a*) *dust storm* for 0.001 mm <ø< 0.1 mm, (*b*) *saltation* for 0.1 mm <ø< 0.5 mm and (*c*) *rolling or surface creep* for 0.5 mm <ø< 1 mm [91,92]. In particular, saltation consists of the bouncing of grains on the ground [93,94]. As reported in literature, the jump produced can reach

significant heights of up to 120 cm, but most jumps do not exceed 30 cm. Jump and impact angles are between 75° and 90° and between 6° and 12° respectively [95]. In desert or semi-desert areas, saltation involves the 55% to 72% of moving particles [91]. Therefore, desert sand moves mostly during spring and summer, when SR and WS reach their maximum values due to the evaporation of interstitial moisture to the desert soil surface [96].

This movement is involved in corrasion. In particular, the plaster begins to detach along the perimeter due to wet-dry cycles and the process is amplified by particles moved by the wind that, through corrasion, tend to abrade the surface between plaster and masonry that has been already partially pulverised due to previous detachment. Given the height reached by particles during saltation, the void generated between the masonry and plaster is most visible in the lower parts of the fragments.

The location of Painted Temple, close to a natural promontory, favours the accumulation of desert sand in the parts of the FN steps. On the steps, whose height varies from 40 to 120 cm, dust and sand particles are accumulated, which, due to wind currents, are continuously moved and erode the decorative apparatus incessantly. The horizontal parts represent the rebound surfaces of saltation grains and, given the heights they reach, the area most vulnerable to this type of degradation is the bottom of the step vertical surface.

The reiteration of such cycles makes initial microcracks evolve into real fractures, as also demonstrated in Dong *et alii* [36] and Luo *et alii* [37]. As shown in Fig. 5c, these can reach a maximum length of 1.5 cm. The growth of fractures induces a reduction of the cohesive surface. Together with the weight loss at the bottom of the steps, new surfaces and borders get constantly exposed to atmospheric agents.

The same degradation processes affecting plasters come into play, although on a smaller scale, for pictorial layers. These are also subjected to wet-dry cycles and subsequent exfoliation and detachment. This weathering is particularly observable on the VR and grisaille-green surfaces. However, *in-situ* observations have shown that the phenomenon is particularly frequent in surface portions where paint layers are stratified. Whenever only a single paint layer is present, in direct contact with the plaster, it is much less intense. This is probably due to the better adhesion of paint layers to the plaster surfaces, which are rough and capable of anchoring the paint. In contrast, in stratified parts, the paint layers are laid on top of each other on very smooth surfaces, which makes adhesion much less effective, thus facilitating exfoliation.

Pulverisation has been observed in PY painted surfaces such as the one shown in the image reported in Fig. 5d. Again, wind erosion and wet-dry cycles are the principal causes. The impacts of particles on the surfaces induces material loss with overall effectiveness depending on the hardness of minerals involved. Nevertheless, the pulverisation of paint layers of Painted Temple can be partially ascribed to the excessive surface drying, which negatively affects the cohesive forces between material particles [97].

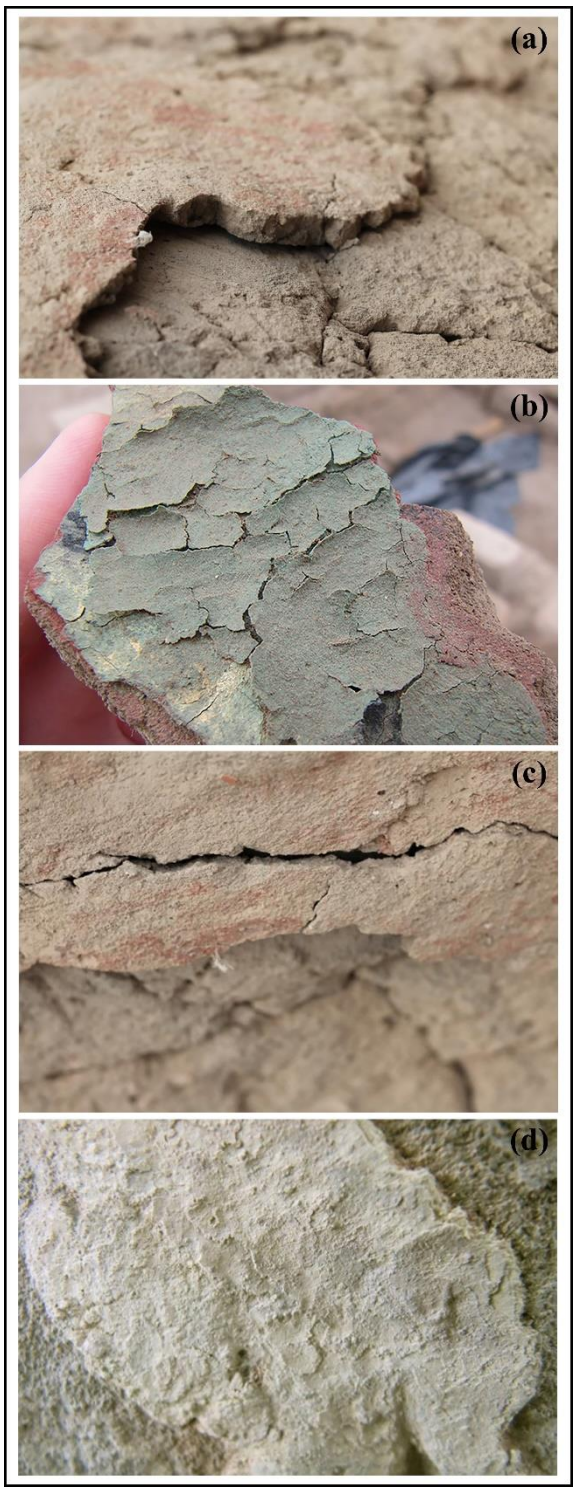

Fig. 5 - (a) Plaster detachment; (b) cracking and exfoliation of the painted surface; (c) a typical fracture in plaster; (d) pulverisation of PY surface.

A surface with very fine particles, as in the case of paint layers, is, in principle, less vulnerable to erosion because of the strong bonds between finer grains [95]. However, the micro-damage generated by repeated impacts can progressively give rise to cracking, peeling and further loss of material.

When the plaster is finally exposed because of painted layer removal by deterioration processes, particle impacts become more effective since clay particles represent a minority constituent, while overall composition consists mainly of silty-sandy particles. These particles are more easily removed during impacts, increasing the speed of the erosion process. For this reason, the borders of paint fragments with relatively well-preserved paint layer exhibit a strong deterioration of the surrounding plaster and, as soon as a void is created between the finishing layers and the wall surface, the fragment detaches.

These processes, in which SR is an extremely important factor, are strongly mitigated by the presence of the shelter and bracing. However, the strong wind, although not directly blowing against the paintwork, is channelled into the area between the surfaces and the bracing and leads to rapid drying.

No degradation attributable to biological activity or factors was observed during the five-years degradation monitoring period.

4.3. Monitoring of decay by STT

Tape analysis reveals that the amount of material removed is closely related to the surface moisture. This depends on solar radiation, T and air circulation, provided that RH is assumed constant during each season. Indeed, all examined archaeological samples, such as the PY subjected to pulverisation shown in Fig. 6a and VR affected by the loss of adhesion between layers shown in Fig. 6b, show that the material is lost mostly during summer, when the surfaces undergo the highest stresses due to rapid drying. The effects can be seen from the image reported in Fig. 6c.

Specifically, PY surfaces, for which more easily cohesion of the paint layer gets reduced and, therefore, appearance is more powdery, show an average material loss of 26.93% ± 1.6 %, in summer. This value decreases in the winter season, when the minimum pictorial loss is 21.44% ± 1.3 %. The material removed by the tape is composed of the smallest grains, which points out a lack of cohesion between particles. For all the surfaces investigated, pulverisation is homogeneous.

VR samples show a maximum average pictorial loss of 13.7% ± 1.4 % in summer and a minimum of 11.46% ± 0.9 % in winter. The range of values is smaller than that measured for the PY surfaces in the same seasons. The VR surfaces are more cohesive but prone to detachment from the underlying layers and the flakes of the paint layer are removed from the surface especially where micro-cracks are present.

The image reported in Fig. 6c clearly shows that PY and VR experience a different material loss. Such difference can be ascribed to differences in the mineralogical composition. In particular, samples with relevant Quartz contents exhibit longer durability than those with similar quartz and clay contents. This correlation between durability and Quartz content is related to the hardness of this mineral. Indeed, according to literature [25], during sand blasting corrasion, colliding bodies cause a damage proportional to their hardness.

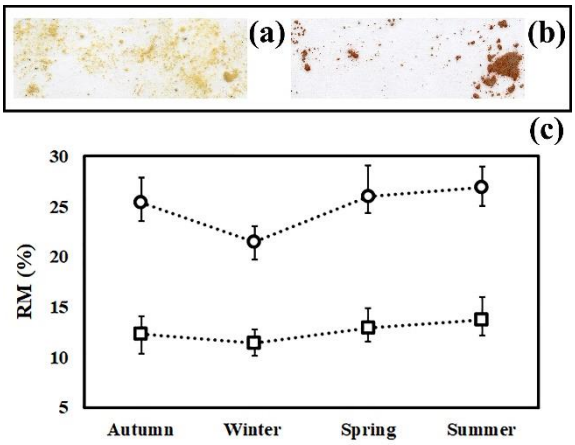

Fig. 6 - (a) STT performed on a PY surface affected by pulverisation; (b) STT performed on VR surface with evident loss of adhesion between layers; (c) Removed material (RM) percentage *vs* seasons. Bars indicates minimum and maximum values of RM. Results have been obtained by STT performed on 7 PY surfaces and 7 VR surfaces (symbols: ○ PY surfaces; □ VR surfaces).

While the considerations made so far are merely qualitative, we pushed the analysis of available data further with the aim of obtaining semi-quantitative correlation between environmental factors and degradation of painted surfaces. Along this way, we noticed that RM% exhibits a significant correlation with T. As shown in Fig. 7a and Fig. 7b, data arrange according to a markedly linear plot with limited scattering around the best-fitted line. It is clear that RM% increases for both PY and VR pigments as T increases. No similar correlation of RM% was observed with other environmental quantities, thus indicating that T is, by far, the most relevant environmental factor affecting the cohesion of the painted layers. The increase of mass loss with temperature can be, indeed, ascribed to a reduction of cohesive forces induced by the removal of water from the material due to the high temperatures it experienced.

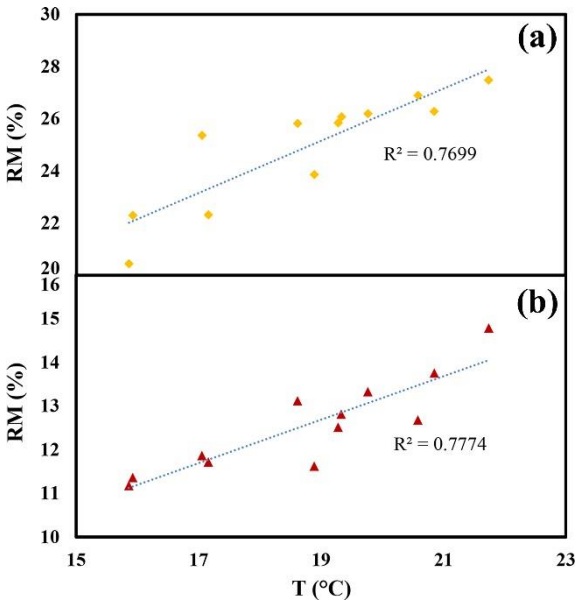

Fig. 7 - (a) Correlation between RM% for PY surfaces (◆) and increased T; (b) Correlation between RM% for VR surfaces (▲) and increased T.

Although temperature can be considered effective itself in damaging the painted layers because of the wet-dry cycles it governs, it is quite reasonable expecting that aeolian processes of significant intensity can worsen the deterioration scenario. For this reason, we have investigated the role of wind strength in some detail. The statistical distribution of WS during one year on the average is shown in Fig. 8. It can be seen that most probable WS values range between 0 and 2.8 m/s. These winds act all over the year and can be regarded as a constant factor of deterioration, even if their low strength cannot be responsible for the most intense degradation phenomena due to saltation. In this respect, a prominent role is played by the strongest winds. As shown in Fig. 8, these have a quite different distribution, their frequency undegoing a seemingly exponential decrease with WS. Quite interestingly, the strongest winds blow exactly during the hot season, thus creating the conditions for a marked impact on painted layer stability, as already noted in Fig. 5.

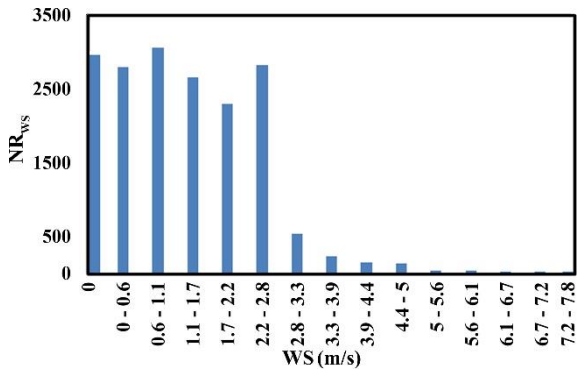

Fig. 8 - Number of records (NRWS) of the different WS ranges during the year.

To highlight the latter aspect, we investigated the coexistence of relatively high temperatures and strong winds. In particular, we checked the monthly days of WS > 2.22 m/s in the presence of T > 20 °C ($ND_{P(\{T;WS\})}$). Data are plotted in Fig. 9. A clear correlation there exists. As a consequence, we can expect that the deterioration process of painted layers is speeded up in specific days of the year, which also discloses a perspective in building a strategy to constrast weathering based on information regarding atmospheric conditions.

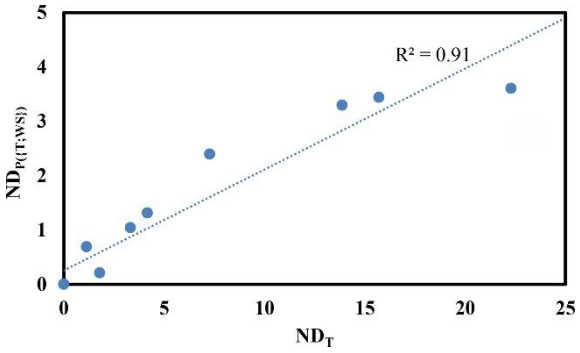

Fig. 9 - Correlation between number of days in the differents months in which a T > 20 °C is associated with a WS > 2.22 m/s ($ND_{P(\{T;WS\})}$) and number of days in the differents months in which T > 20 °C(ND_T).

A further evidence of how important is the combination of high temperatures and strong winds come from the plots in Fig. 10, where the RM% values for the two pigments PY and VR are compared, month by month, with the number of days in which WS > 2.22 m/s in the presence of T > 20 °C. The correlation between the two quantities is straightforward. Our data confirm, on a quantitative basis, that painted surfaces undergo most intense deterioration processes when high temperatures combine with great wind strengths.

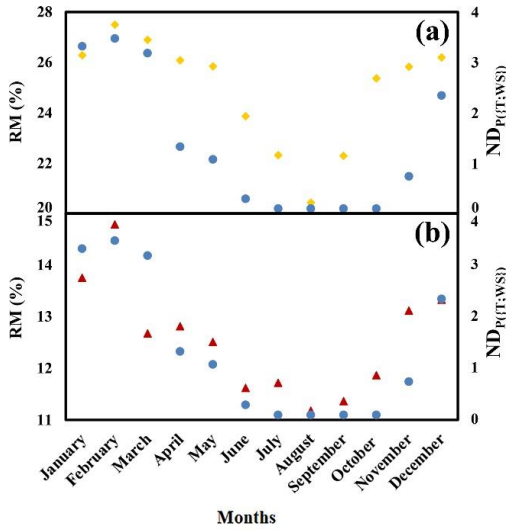

Fig. 10 - (a) Correlation between RM% for PY surfaces (🔸) and $ND_{P(\{T;WS\})}$(🔵); (b) Correlation between RM% for VR surfaces (🔺) and $ND_{P(\{T;WS\})}$ (🔵).

5. Conclusions

This work investigated damaging phenomena of Painted Temple caused by environmental and climatic features. The seasonal variation of atmospheric conditions results in the damage of painted layers due to the combination of multiple simultaneous and synergistic deterioration processes. According to our data, the prominent role in surface degradation is played by temperature, wet-dry, wind activity cycles. Specifically, a linear correlation between the amount of material loss and the ambient temperature has been observed. This is clear evidence that the painted plasters decrease their cohesion as the temperature rises.

It is also evident that the highest temperatures are often observed in combination with the strongest winds. Indeed, the deterioration processes intensify and the surface layers exhibit enhanced mass loss.

As a whole, our work shows the importance of systematic investigation over long observation periods and the need of relating environmental information with careful monitoring in situ of endangered materials.

Although not conclusive, the proposed work highlights the need to evaluate a large number of parameters that together can contribute to the degradation of materials in operation. In particular, the collection of data and their correlation will support researchers in the materials science field to develop predictive models of degradation kinetics based on environmental and climatic observations.

References

[1] G. De La Vega, Comentarios reales. Origen e Historia de los Incas del Peru (1609), Mercurio, Lima, 1970.

[2] D. Pozzi-Escot, G. Pacheco, C.R. Uceda, Pachacamac: Templo Pintado.Conservacion e Investigación, (2013).

[3] U. Lohmann, R. Sausen, L. Bengtsson, U. Cubasch, J. Perlwitz, E. Roeckner, The Koppen climate classification as a diagnostic tool for general circulation models, Clim. Res. 3 (1993) 177–193. https://doi.org/10.3354/cr003177.

[4] M. Kottek, J. Grieser, C. Beck, B. Rudolf, F. Rubel, World map of the Köppen-Geiger climate classification updated, Meteorol. Zeitschrift. 15 (2006) 259–263. https://doi.org/10.1127/0941-2948/2006/0130.

[5] H.E. Beck, N.E. Zimmermann, T.R. McVicar, N. Vergopolan, A. Berg, E.F. Wood, Present and future köppen-geiger climate classification maps at 1-km resolution, Sci. Data. 5 (2018) 1–12. https://doi.org/10.1038/sdata.2018.214.

[6] M.C. Peel, B.L. Finlayson, T.A. McMahon, Updated world map of the Köppen-Geiger climate classification, Hydrol. Earth Syst. Sci. Discuss. 11 (2007) 1633–1644. https://hal.science/hal-00305098/document.

[7] D. Pozzi-Escot, Pachacamac: Conservación en arquitectura de tierra, Ministerio de Cultura, Lima, 2014.

[8] D. Pozzi-Escot, Santuario arqueológico Pachacamac, Lima, 2016.

[9] P. Paredes Botoni, La Huaca pintada o el templo de Pachacamac, Bol. Lima. 41 (1985) 70–84.

[10] D. Pozzi-Escot, G. Pacheco, C.R. Uceda, Pachacamac: Templo Pintado - Conservación e Investigación, Ministerio, Lima, 2013.

[11] R. Franco Jordán, Poder religioso , crisis y prosperidad en Pachacamac : del Horizonte Medio al Intermedio, Bull. l ' Inst. Français d ' Études Andin. 33 (2004) 1–46.

[12] D. Bonavia, Pinturas murales Mochicas: algunas consideraciones, Hist. Lima. VIII (1984) 89–95.

[13] G. Marcone Flores, Los murales del Templo Pintado o Relación entre el Santuario de Pachacamac y la iconografía tardía de la Costa Central Peruana, An. Del Mus. Am. 11 (2003) 57–80.

[14] J.C. Muelle, R. Wells, Las pinturas del Templo de Pachacamac, Rev. Del Mus. Nac. 8 (1939) 265–282.

[15] D. Bonavia, Ricchata Quellccani, Fondo del, Lima, 1974.

[16] R.P. Schaedel, Mochica Murals at Pañamarca, Archaeology. 4 (1951) 145–154.

[17] R. Franco Jordán, C. Gálvez, S. Vásquez, Arquitectura y decoración mochica en la Huaca

Cao Viejo, Complejo El Brujo: resultados preliminares, in: U.N. de la L.– T. Institut français d'études andines (Ed.), Moche Propuestas y Perspect., Lima, 1994: pp. 147–180. https://doi.org/10.4000/books.ifea.2367.

[18] R. Franco Jordán, C. Gálvez, S. Vásquez, Modelos, función y cronología en la Huaca Cao Viejo, complejo El Brujo, in: S. Uceda, E. Mujica (Eds.), Moche Hacia El Final Del Milen. Actas Del Segundo Coloq. Sobre La Cult. Moche (Trujillo, 1 Al 7 Agosto 1999), Universidad Nacional de Trujillo y Pontificia Universidad Católica del Perú, 2003: pp. 125–178.

[19] C. Campana, R. Morales, Historia de una deidad mochica, Lima, 1997.

[20] V. Wright, Pigmentos y tecnología artística mochicas: una nueva aproximación en la comprensión de la organización social, Bull. l'Institut Français d'études Andin. 39 (2010) 299–330. https://doi.org/10.4000/bifea.1950.

[21] M. Sepúlveda, V. Wright, Capítulo 17. Pigmentos, pinturas rupestres y murales, in: U. de T. Institut français d'études andines, Université Bordeaux Montaigne (Ed.), ARQUEOMETRÍA. Estud. Analíticos Mater. Arqueol., Lima, 2018: pp. 369–392.

[22] M. Shao, L. Li, S. Wang, E. Wang, Z. Li, Deterioration mechanisms of building materials of Jiaohe ruins in China, J. Cult. Herit. 14 (2013) 38–44. https://doi.org/10.1016/j.culher.2012.03.006.

[23] D. Ogura, T. Hase, Y. Nakata, A. Mikayama, S. Hokoy, H. Takabayashi, K. Okada, B. Su, P. Xue, Influence of Environmental Factors on Deterioration of Mural Paintings in Mogao Cave 285, Dunhuang, in: J.M.P.Q. Delgado (Ed.), Case Stud. Build. Rehabil. Build. Pathol. Rehabil., Porto, 2021: pp. 105–159. http://www.springer.com/series/10019.

[24] X. He, M. Xu, H. Zhang, B. Zhang, B. Su, An exploratory study of the deterioration mechanism of ancient wall-paintings based on thermal and moisture expansion property analysis, J. Archaeol. Sci. 42 (2014) 194–200. https://doi.org/10.1016/j.jas.2013.10.035.

[25] M. Cappai, L. Casnedi, G. Carcangiu, F. Delogu, D. Pozzi-escot, G. Pacheco, G. Pia, P. Meloni, Weathering of earth-painted surfaces : Environmental monitoring and artificial aging, Constr. Build. Mater. 344 (2022) 128193. https://doi.org/10.1016/j.conbuildmat.2022.128193.

[26] K.A. Heathcote, Durability of earthwall buildings, Constr. Build. Mater. 9 (1995) 185–189.

https://doi.org/10.1016/0950-0618(95)00035-E.

[27] J.C. Morel, Q.B. Bui, E. Hamard, Weathering and durability of earthen material and structures, in: Mod. Earth Build. Mater. Eng. Constr. Appl., 2012: pp. 282–303. https://doi.org/10.1533/9780857096166.2.282.

[28] M. Torres-González, C. Rubio-Bellido, D. Bienvenido-Huertas, J.M. Alducin-Ochoa, V. Flores-Alés, Long-term environmental monitoring for preventive conservation of external historical plasterworks, J. Build. Eng. 47 (2022). https://doi.org/10.1016/j.jobe.2021.103896.

[29] M. Correia, L. Guerrero, A. Crosby, Technical strategies for conservation of Earthen archaeological architecture, Conserv. Manag. Archaeol. Sites. 17 (2015) 224–256. https://doi.org/10.1080/13505033.2015.1129799.

[30] L. Guerrero, M. Correia, H. Guillaud, Conservación del patrimonio arqueológico construido con tierra en iberoamérica., Conserv. Ibero-American Archaeol. Herit. Built Earth. 25 (2012) 210–225. http://ezproxy.uniandes.edu.co:8080/login?url=http://search.ebscohost.com/login.aspx?direct=true&db=fua&AN=91642368&lang=es&site=eds-live&scope=site.

[31] F. Matero, Conservation and Management of Archaeological Sites Mud Brick Metaphysics and the Preservation of Earthen Ruins Mud Brick Metaphysics and the Preservation of Earthen Ruins, Conserv. Manag. Archaeol. Sites. 17 (2016) 209–223. https://doi.org/10.1080/13505033.2015.1129798.

[32] M. Oliver, A. Mesbah, Behaviour of ancient and new structures made out of raw earth, Trans. Built Environ. 4 (1998). https://www.witpress.com/Secure/elibrary/papers/STR93/STR93042FU.pdf.

[33] C.T.S. Beckett, P.A. Jaquin, J.C. Morel, Weathering the storm: A framework to assess the resistance of earthen structures to water damage, Constr. Build. Mater. 242 (2020) 1–12. https://doi.org/10.1016/j.conbuildmat.2020.118098.

[34] H. Hugo, H. Guillard, Earth Construction: A Comprehensive Guide, 1994.

[35] H. Houben, A.A. Balderrama, Our Earthen Architectural Heritage : Materials Conservation Raw Earth Construction, MRS Bull. 29 (2004) 338–341. www.mrs.org/publications/bulletin.

[36] M. Dong, H. Hu, Q. Guo, X. Gong, R. Azzam, M. Kong, Correlation of environmental parameters and the water saturation induced deterioration of earthen archaeological sites: The

case of world heritage Liangzhu city, China, Heritage. 4 (2021) 387–400. https://doi.org/10.3390/heritage4010024.

[37] X. Luo, Z. Gu, C. Yu, Desiccation cracking of earthen sites in archaeology museum - A viewpoint of chemical potential difference of water content, Indoor Built Environ. 24 (2015) 147–152. https://doi.org/10.1177/1420326X15570810.

[38] H. Barnard, W.Z. Wendrich, A. Winkels, J.E.M.F. Bos, B.L. Simpson, R.T.J. Cappers, The preservation of exposed mudbrick architecture in Karanis (Kom Aushim), Egypt, J. F. Archaeol. 41 (2016) 84–100. https://doi.org/10.1080/00934690.2015.1131109.

[39] L. Casnedi, M. Cappai, A. Cincotti, F. Delogu, G. Pia, Porosity effects on water vapour permeability in earthen materials : Experimental evidence and modelling description, J. Build. Eng. 27 (2020) 100987. https://doi.org/10.1016/j.jobe.2019.100987.

[40] F.G. Matero, The Conservation of Plasters in Earthen Archeological Sites, in: Conserv. Earthen Archit., 1999: pp. 59–62.

[41] L.F. Guerrero Baca, Revoques para la conservación de obras arqueológicas de tierra en Mexico, in: T. Joffroy, H. Guillard, C. Sadozaï (Eds.), Terra Lyon 2016 Actes / Proc. / Actos, CRATerre, Villefontaine, 2017: pp. 94–98.

[42] A. Weyer, P. Roig Picazo, D. Pop, J. Cassar, A. Özköse, J. Vallet, I. Srša, EwaGlos – European Illustrated Glossary of Conservation Terms for Wall Paintings and Architectural Surfaces, 2015.

[43] C. Atzeni, G. Pia, U. Sanna, N. Spanu, Surface wear resistance of chemically or thermally stabilized earth-based materials, Mater. Struct. 41 (2008) 751–758. https://doi.org/10.1617/s11527-007-9278-1.

[44] R.J. Carr, Evaluation of Adhesive Binders for the Preservation of In-Situ Aboriginal Surface Finishes at Mesa Verde National Park Evaluation of Adhesive Binders for the Preservation of In-Situ Aboriginal Surface Finishes at Mesa Verde National Park, University of Pennsylvania, 2002.

[45] L. Rainer, The conservation of decorated architectural surfaces, Getty Conserv. Inst. Newsl. 25 (2010) 1–9. http://getty.edu/conservation/publications_resources/newsletters/25_2/feature.html.

[46] W. Chen, Y. Zhang, J. Zhang, P. Dai, Consolidation effect of composite materials on earthen

sites, Constr. Build. Mater. 187 (2018) 730–737. https://doi.org/10.1016/j.conbuildmat.2018.07.239.

[47] A. Ferron, F.G. Matero, A Comparative Study of Ethyl-silicate–based Consolidants on Earthen Finishes, J. Am. Inst. Conserv. 50 (2013) 49–72. https://doi.org/10.1179/019713611804488964.

[48] C.D. Kaplan, F. Murtezaoğlu, B. Ipekoğlu, H. Böke, Weathering of andesite monuments in archaeological sites, J. Cult. Herit. 14 (2013) 77–83. https://doi.org/10.1016/j.culher.2012.11.022.

[49] M. Heidari, M. Torabi-Kaveh, C. Chastre, M. Ludovico-Marques, H. Mohseni, H. Akefi, Determination of weathering degree of the Persepolis stone under laboratory and natural conditions using fuzzy inference system, Constr. Build. Mater. 145 (2017) 28–41. https://doi.org/10.1016/j.conbuildmat.2017.03.230.

[50] A.J. Prieto, A. Silva, J. de Brito, J.M. Macías-Bernal, F.J. Alejandre, Multiple linear regression and fuzzy logic models applied to the functional service life prediction of cultural heritage, J. Cult. Herit. 27 (2017) 20–35. https://doi.org/10.1016/j.culher.2017.03.004.

[51] A. Agapiou, V. Lysandrou, D.D. Alexakis, K. Themistocleous, B. Cuca, A. Argyriou, A. Sarris, D.G. Hadjimitsis, Cultural heritage management and monitoring using remote sensing data and GIS: The case study of Paphos area, Cyprus, Comput. Environ. Urban Syst. 54 (2015) 230–239. https://doi.org/10.1016/j.compenvurbsys.2015.09.003.

[52] L.R. Gobakken, J. Mattsson, G. Alfredsen, In-service performance of wood depends upon the critical in-situ conditions . Case studies ., Proc. IRG Annu. Meet. IRG/WP (2008) 13.

[53] A.R. Young, The Rietveld Method, Oxford Science Pubblication, New York, 2000.

[54] D.M. Moore, R.C. Reynolds, X-ray Diffraction and the Identification and Analysis of Clay Minerals, Oxford University Press, New York, 1997.

[55] UNI, EN ISO 14688-1:2018 - Geotechnical investigation and testing - Identification and classification of soil - Part 1: Identification and description, (2018).

[56] UNI, UNI EN ISO 17892-4:2017 - Geotechnical investigation and testing - Laboratory testing of soil - Part 4: Determination of particle size distribution, 2017.

[57] P. Mora, G. Torraca, Fissativi per dipinti murali, in: Boll. ICR, Rome, 1965: pp. 109–132.

[58] P. Mora, L. Mora, P. Philippot, Conservation of wall paintings, London, 1984.

[59] A. Ferron, The Consolidation of Earthen Surface Finishes : A Study of Disaggregating Plasters at Mesa Verde National Park, University of Pennsylvania, 2007.

[60] K. Catenazzi, Evaluation of the use of Funori for consolidation of powdering paint layers in wall paintings, Stud. Conserv. 62 (2017) 96–103. https://doi.org/10.1080/00393630.2015.1131043.

[61] G. Pacheco, D. Pozzi-escot, M. Cappai, S. Malpartida Tuncar, S. Petrick, Productos orgánicos para la conservación de pintura mural, in: T. Joffroy, H. Guillaud, S. Chamsia (Eds.), Terra Lyon 2016 Actes / Proc. / Actos, CRATerre, Villefontaine, 2018: pp. 133–137.

[62] S. Malpartida Tuncar, Estudio de algunas propiedades físicas de enlucidos de barro consolidados con mucílago de tuna, agar agar y gelatina, Universidad Nacional de Ingeniería, Lima, Peru, 2015. http://cybertesis.uni.edu.pe/handle/uni/4536.

[63] M. Drdácký, J. Lesák, S. Rescic, Z. Slížková, P. Tiano, J. Valach, Standardization of peeling tests for assessing the cohesion and consolidation characteristics of historic stone surfaces, Mater. Struct. Constr. 45 (2012) 505–520. https://doi.org/10.1617/s11527-011-9778-x.

[64] I. Natali, P. Tomasin, F. Becherini, A. Bernardi, C. Ciantelli, M. Favaro, O. Favoni, V.J.F. Pérez, I.D. Olteanu, M.D.R. Sanchez, A. Vivarelli, A. Bonazza, Innovative consolidating products for stone materials: Field exposure tests as a valid approach for assessing durability, Herit. Sci. 3 (2015) 1–13. https://doi.org/10.1186/s40494-015-0036-3.

[65] A. Bonazza, G. Vidorni, I. Natali, C. Ciantelli, C. Giosuè, F. Tittarelli, Durability assessment to environmental impact of nano-structured consolidants on Carrara marble by field exposure tests, Sci. Total Environ. 575 (2017) 23–32. https://doi.org/10.1016/j.scitotenv.2016.10.004.

[66] M. Drdácký, J. Lesák, K. Niedoba, J. Valach, Peeling tests for assessing the cohesion and consolidation characteristics of mortar and render surfaces, Mater. Struct. Constr. 48 (2015) 1947–1963. https://doi.org/10.1617/s11527-014-0285-8.

[67] R. Giorgi, L. Dei, P. Baglioni, A New Method for Consolidating Wall Paintings Based on Dispersions of Lime in Alcohol Rodorico Giorgi , Luigi Dei and Piero Baglioni Source : Studies in Conservation , Vol . 45 , No . 3 (2000), pp . 154-161 Published by : Taylor & Francis, 45 (2018) 154–161.

[68] P. Faria, T. Santos, J.E. Aubert, Experimental characterization of an earth eco-efficient

plastering mortar, J. Mater. Civ. Eng. 28 (2016). https://doi.org/10.1061/(ASCE)MT.1943-5533.0001363.

[69] T. Santos, P. Faria, Evaluating earthen mortars for rendering, in: C. JOFFROY, Thierry, GUILLAUD, Hubert, SADOZAÏ (Ed.), Terra Lyon 2016 Actes / Proc. / Actos, CRATerre, Villefontaine, 2018: pp. 1–7. https://craterre.hypotheses.org/files/2018/05/TERRA-2016_Th-4_Art-416_Santos.pdf.

[70] ASTM, ASTM 4214-07 - Standard Test Methods for Evaluating the Degree of Chalking of Exterior Paint Films, (2015).

[71] Ente Nazionale Italiano di Unificazione, UNI EN ISO 4628-6:2011, (2011).

[72] G.M. Reeves, I. Sims, J.C. Cripps, eds., Clay Materials Used in Construction, Geological Society, London, 2006. https://doi.org/10.16309/j.cnki.issn.1007-1776.2003.03.004.

[73] A.M. Forster, G.M. Medero, T. Morton, J. Buckman, Traditional cob wall: Response to flooding, Struct. Surv. 26 (2008) 302–321. https://doi.org/10.1108/02630800810906557.

[74] I.R. Killip, D.W. Cheetham, The prevention of rain penetration through external walls and joints by means of pressure equalization, Build. Environ. 19 (1984) 81–91. https://doi.org/10.1016/0360-1323(84)90033-7.

[75] J. He, W. Zhou, D. Hu, S. Liu, J. Otero, C. Rodriguez-Navarro, A multi-analytical approach for the characterization of materials, manufacturing process and damage mechanisms of wall paintings in Samye Temple, Tibet, Dye. Pigment. 207 (2022) 110704. https://doi.org/10.1016/j.dyepig.2022.110704.

[76] K. Elert, C. Rodriguez-Navarro, Degradation and conservation of clay-containing stone: A review, Constr. Build. Mater. 330 (2022) 127226. https://doi.org/10.1016/j.conbuildmat.2022.127226.

[77] C. Rodriguez-Navarro, E. Sebastian, E. Doehne, W.S. Ginell, The role of sepiolite-palygorskite in the decay of ancient Egyptian limestone sculptures, Clays Clay Miner. 46 (1998) 414–422. https://doi.org/10.1346/CCMN.1998.0460405.

[78] M. Müller-Vonmoos, T. Løken, The swelling behaviour of clays, Appl. Clay Sci. 4 (1989) 125–141. https://doi.org/10.1016/0169-1317(89)90004-5.

[79] Y. Du, K. Cui, S. Chen, W. Dong, W. Chen, Quantitative research on the development

difference of scaling off on the sunward side and nightside of earthen sites, J. Cult. Herit. 57 (2022) 107–117. https://doi.org/10.1016/j.culher.2022.08.008.

[80] A. Alva Balderrama, G. Chiari, Protection and Conservation of Excaved Structures of Mudbrick, in: ICCROM (Ed.), Conserv. Archaeol. Excav. Part. Ref. to Mediterr. Area, 2° ed., N. P. STANLEY PRICE, Rome, 1995: pp. 101–112.

[81] L. Cooke, Conservation Approaches to Earthen Architecture in Archaeological Contexts, British Ar, Oxford, 2010.

[82] D. Camuffo, Microclimate for cultural heritage - Conservation, Restaoration, and Maintenance of Indoor and Outdoor Monuments, 2° ed., 2014.

[83] K.A. Heathcote, An investigation Into the erodibility of earth wall units - PhD Thésis, University of Technology, Sidney, (2002) 272. https://opus.lib.uts.edu.au/bitstream/2100/241/2020/02Whole.pdf.

[84] C.L. Zhang, X.Y. Zou, J.R. Gong, L.Y. Liu, Y.Z. Liu, Aerodynamic roughness of cultivated soil and its influences on soil erosion by wind in a wind tunnel, Soil Tillage Res. 75 (2004) 53–59. https://doi.org/10.1016/S0167-1987(03)00159-4.

[85] D.E. Buschiazzo, T.M. Zobeck, S.A. Abascal, Wind erosion quantity and quality of an Entic Haplustoll of the semi-arid pampas of Argentina, J. Arid Environ. 69 (2007) 29–39. https://doi.org/10.1016/j.jaridenv.2006.08.013.

[86] M. V. López, Wind erosion in agricultural soils: An example of limited supply of particles available for erosion, Catena. 33 (1998) 17–28. https://doi.org/10.1016/S0341-8162(98)00064-2.

[87] L. Gomes, J.L. Arrúe, M. V. López, G. Sterk, D. Richard, R. Gracia, M. Sabre, A. Gaudichet, J.P. Frangi, Wind erosion in a semiarid agricultural area of Spain: The WELSONS project, Catena. 52 (2003) 235–256. https://doi.org/10.1016/S0341-8162(03)00016-X.

[88] C. Atzeni, F. Bodano, U. Sanna, N. Spanu, Surface strength: definition and testing by a sand impact method, J. Cult. Herit. 7 (2006) 201–205. https://doi.org/10.1016/j.culher.2006.05.002.

[89] R. Striani, M. Cappai, L. Casnedi, C. Esposito Corcione, G. Pia, Coating's influence on wind erosion of porous stones used in the Cultural Heritage of Southern Italy: Surface characterisation and resistance, Case Stud. Constr. Mater. 17 (2022) e01501.

https://doi.org/10.1016/j.cscm.2022.e01501.

[90] D.A. Gillette, I.H. Blifford Jr, C.R. Fenster, Measurements of Aerosol Size Distributions and Vertical Fluxes of Aerosols on Land Subject to Wind Erosion, J. Appl. Meteorol. 11 (1972) 977–987.

[91] W.S. Chepil, Dynamics of wind erosion: I.Nature of movement of soil by wind, Soil Sci. 60 (1945) 305–320.

[92] S. Zamani, M. Mahmoodabadi, Effect of particle-size distribution on wind erosion rate and soil erodibility, Arch. Agron. Soil Sci. 59 (2013) 1743–1753. https://doi.org/10.1080/03650340.2012.748984.

[93] D. Camuffo, Controlling the aeolian erosion of the Great Sphinx, Stud. Conserv. 38 (1993) 198–205. https://doi.org/10.2307/1506380.

[94] D. Camuffo, Physical weathering of stones, Sci. Total Environ. 167 (1995) 1–14. https://doi.org/10.1016/0048-9697(95)04565-I.

[95] Y. Hao, Y. Feng, J. Fan, Experimental study into erosion damage mechanism of concrete materials in a wind-blown sand environment, Constr. Build. Mater. 111 (2016) 662–670. https://doi.org/10.1016/j.conbuildmat.2016.02.137.

[96] W.S. Chepil, Properties of soil which influence wind erosion : IV . State of dry aggregate structure, Soil Sci. 72 (1851) 387–401.

[97] B. Fletcher, The incipient motion of granular materials, J. Phys. D. Appl. Phys. 9 (1976) 913–924.